ELSEVIER

Journal of Power Sources 86 (2000) 423–431

JOURNAL OF POWER SOURCES

www.elsevier.com/locate/jpowsour

Evaluation and modeling of performance of anode-supported solid oxide fuel cell

H. Yakabe *, M. Hishinuma, M. Uratani, Y. Matsuzaki, I. Yasuda

Fundamental Technology Laboratory, Tokyo Gas, 16-25, Shibaura, 1-chome, Minato-ku, Tokyo 105-0023, Japan

Accepted 18 October 1999

Abstract

For an anode-supported planar SOFC, a single-unit with double channels was modeled for a counter-flow pattern, and the concentration polarization at the anode was estimated. The flow phenomena were simulated using the finite volume method and the distribution of the gaseous species was calculated. In the model, it was assumed that the gas flow in the porous anode is governed by Darcy's Law, and the reactant species are transported to the electrolyte/anode interface mainly by diffusion in a multicomponent mixture system. For binary H_2–H_2O and CO–CO_2 systems, the calculated concentration polarization was found comparable to the experimental results. As an example for a multicomponent system, a model using steam-reformed methane as a fuel was employed to simulate the concentration polarization at a high fuel utilization. From the simulated results, it was evident that the shift reaction effectively reduces the concentration polarization when the fuel utilization is high.

Keywords: Solid oxide fuel cell; Anode-supported cell; Concentration polarization; Modeling; Diffusion of gases

1. Introduction

Anode-supported solid oxide fuel cells (SOFCs) are receiving considerable interest since they are suited for operation at lower temperatures [1]. By lowering the operating temperature of the SOFCs to around 700°C, conventional stainless steel can be used for interconnectors or auxiliary components with which high mechanical reliability of a cell-stack and lower manufacturing costs can be achieved. For the anode-supported cell, it is advantageous that the ohmic resistance is lower than that of the electrolyte-supported cell because much thinner electrolyte films can be employed. However, the contribution of the concentration polarization to voltage losses at high current densities will be significant since the thick anode prevents the supply of reactant gases to the electrochemical reaction sites at the anode/electrolyte interface. In thick porous anodes, the momentum of fuel gas is nearly zero and the fuel supply to the electrolyte is carried out mainly by diffusion of the reactant species [2]. Accordingly, the electrode reaction at the electrolyte/anode interface is governed by the rate of the reactant diffusion when the current density or the fuel utilization is high. The diffusion rates of the reactant gases in the anode are affected by the structural nature of the anode, e.g., the pore size, the volume fraction of the pores, and the tortuosity. In addition, they depend on the type of the individual reactant and the whole fuel gas composition. The feed rate of the reactant gas to the electrolyte is a function of the position along the fuel flow over the anode, and, thus, the concentration polarization is not the same throughout the anode. The experimentally measured concentration polarization will be the average value over the anode at a high current density and a high fuel utilization. Thus, it is helpful to model the performance of the anode-supported cell and calculate the distribution of the concentration polarization at the anode in order to understand the effects of the gas composition and the anode structure on the concentration polarization.

In the present study, we constructed a three-dimensional model to estimate the cell performance. A simplified single-unit model with bipolar channels for a counter-flow pattern was employed, and the distribution of the gas species and the concentration polarization at the anode were calculated. The concentration polarization was estimated for various fuel gas compositions and current densi-

* Corresponding author

0378-7753/00/$ - see front matter
PII: S0378-7753(99)00444-9

ties, and the simulated results were compared with the experimentally obtained data.

2. Mathematical model

We modelled a single-unit with bipolar channels in the one-cell stack and simulated the concentration overpotential η_c. The one-cell stack and the single-unit model are illustrated in Fig. 1. For the sake of simplicity in the calculation, we analyzed half of the one repeating unit in the centre part of the one-cell stack. The thermofluid analysis was carried out using the finite-volume method.

In the model, in addition to the electrochemical reactions

(at electrolyte/anode interface)

$$H_2 + O^{2-} \rightarrow H_2O + 2e^- \quad (1)$$

$$CO + O^{2-} \rightarrow CO_2 + 2e^- \quad (2)$$

(at cathode)

$$1/2O_2 + 2e^- \rightarrow O^{2-}, \quad (3)$$

the following shift reaction was taken into account:

$$H_2O + CO \leftrightarrow H_2 + CO_2. \quad (4)$$

The electrochemical reactions were assumed to be instantaneous at both electrodes and occur at the interfaces between electrodes and electrolyte. The shift reaction was supposed to be in chemical equilibrium at any point in the anode.

For the flow analysis in the porous anode, it was assumed from Darcy's Law [3] that within the volume

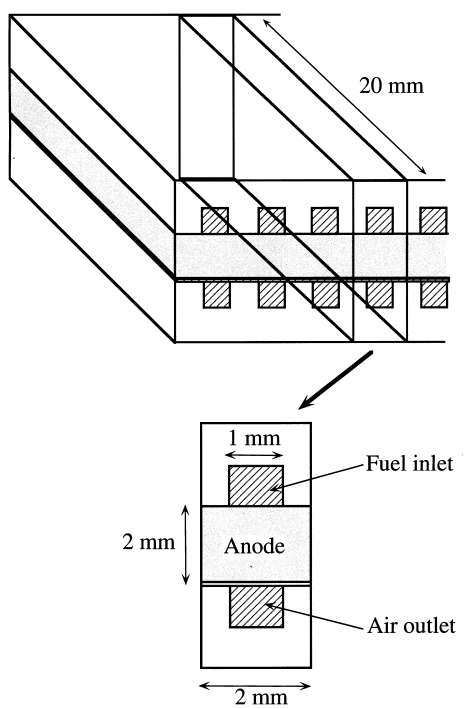

Fig. 1. Schematic diagram of the one cell stack and the single-unit cell model for the anode-supported SOFC.

Table 1
List of the Lennard–Jones potentials used in the simulation

	Gas species							
	N_2	O_2	CH_4	H_2O	CO	H_2	CO_2	Ar
σ_i[a]	3.798	3.467	3.758	2.641	3.690	2.827	3.941	3.542
ε_i[a]	71.4	106.7	148.6	809.1	91.7	59.7	195.2	93.3

[a] Taken from Ref. [6].

containing the distributed resistance, a local balance should be maintained between pressure and resistance forces such that

$$-K_i u_i = \frac{\partial p}{\partial \xi_i} \quad (5)$$

where ξ_i $(i = 1, 2, 3)$ represents the orthotropic direction, p is the pressure, and K_i and u_i are, respectively, the permeability and the superficial velocity in direction ξ_i.

Using the parallel pore model [4], the effective gas diffusion coefficient for component i in the porous media can be expressed as follows:

$$D_{ie} = \frac{\varepsilon}{\tau}\left(\frac{1 - \alpha_{im} y_i}{D_{i,m}} + \frac{1}{D_{Ki}}\right)^{-1} \quad (6)$$

where ε is the volume fraction of pores, τ is the tortuosity factor, $D_{i,m}$ is the molecular diffusion coefficient of the component i, y_i is the molar fraction, and D_{Ki} is the Knudsen diffusion coefficient. α_{im} is defined as

$$\alpha_{im} = 1 - \left(\frac{M_i}{M_m}\right)^{1/2} \quad (7)$$

where M_i is the molecular weight of the component i, and M_m is the average molecular weight.

The Knudsen diffusion coefficient for the component i in the multicomponent mixture gas is written by

$$D_{Ki} = \frac{2}{3}\left(\frac{8RT}{\pi M_i}\right)^{1/2} \bar{r} \quad (8)$$

where R is the gas constant, T is the gas temperature, and r is the average radius of the pore [4]. In a multicomponent gas system, the molecular diffusion coefficient of the component i is given by

$$D_{i,m} = \frac{1 - y_i}{\sum_{k \neq i} \frac{y_k}{D_{ik}}} \quad (9)$$

where D_{ik} is the binary diffusion coefficient in the system having components i and k [5]. Using the first order

Table 2
List of the parameters related to structural nature of the anode substrate

Porosity (%)	Average pore size (μm)	Tortuosity	Permeability of anode ($m^2\ Pa^{-1}\ s^{-1}$)
46[a]	2.6[a]	4.5	1.7×10^{-10}[a,b]

[a] Experimentally measured value.
[b] Measured using N_2 gas at room temperature.

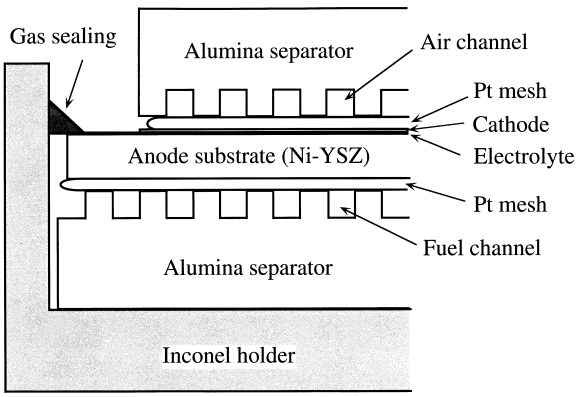

Fig. 2. Schematic diagram of the layout for the concentration overpotential measurement.

equation in Chapman–Enskog theory, the binary diffusion coefficient D_{ik} is derived as follows [6],

$$D_{ik} = 0.001858 \frac{\left[T^3(M_i + M_k)/M_i M_k\right]^{1/2}}{p\sigma_{ik}^2 \Omega_D} \quad (10)$$

where σ_{ik} is the characteristic length, and Ω_D is the collision integral. Using the Lennard–Jones 12–6 potential model [7], Ω_D is given by

$$\Omega_D = \frac{A}{T_N^B} + \frac{C}{\exp(DT_N)} + \frac{E}{\exp(FT_N)} + \frac{G}{\exp(HT_N)} \quad (11)$$

where the constants A to H are $A = 1.06036$, $B = 0.15610$, $C = 0.19300$, $D = 0.47635$, $E = 1.03587$, $F = 1.52996$, $G = 1.76474$, $H = 3.89411$, and T_N is defined by

$$T_N = \frac{kT}{\varepsilon_{ik}} \quad (12)$$

where k is the Boltzmann constant and ε_{ik} is the characteristic Lennard–Jones energy. From the usually employed simple rules [8], σ_{ik} and ε_{ik} are given by,

$$\sigma_{ik} = \frac{\sigma_i + \sigma_k}{2}$$

$$\varepsilon_{ik} = (\varepsilon_i \varepsilon_k)^{1/2} \quad (13)$$

where σ_i is the diameter of the molecular collision. The parameters used for the calculation of $D_{i,m}$ in the simulation are listed in Table 1.

Using the Nernst equation, the concentration overpotential η_c was defined as follows,

$$\eta_c = \frac{RT}{4F} \ln \frac{p^0_{O_2}}{p_{O_2(a)}} \quad (14)$$

where F is the Faraday constant, $p^0_{O_2}$ is the partial pressure of oxygen in the bulk of the fuel stream, $p_{O_2(a)}$ is the partial pressure of oxygen at the electrolyte/anode interface. The cell operating temperature in the model was set to 750°C.

The cell performance of the anode-supported cell was experimentally measured in H_2–H_2O and CO–CO_2 systems at 750°C. The single anode-supported cell used for the measurement was prepared by co-firing a NiO-8YSZ substrate dip-coated with 8YSZ slurry at 1400°C. For the cathode, a composite of $Pr_{0.6}Sr_{0.4}MnO_3$ and $Ce_{0.8}Sm_{0.2}O_{1.9}$ was screen-printed onto the electrolyte and fired at 1150°C. The anode thickness after the co-firing was about 2 mm. The parameters for the simulation related to the structural

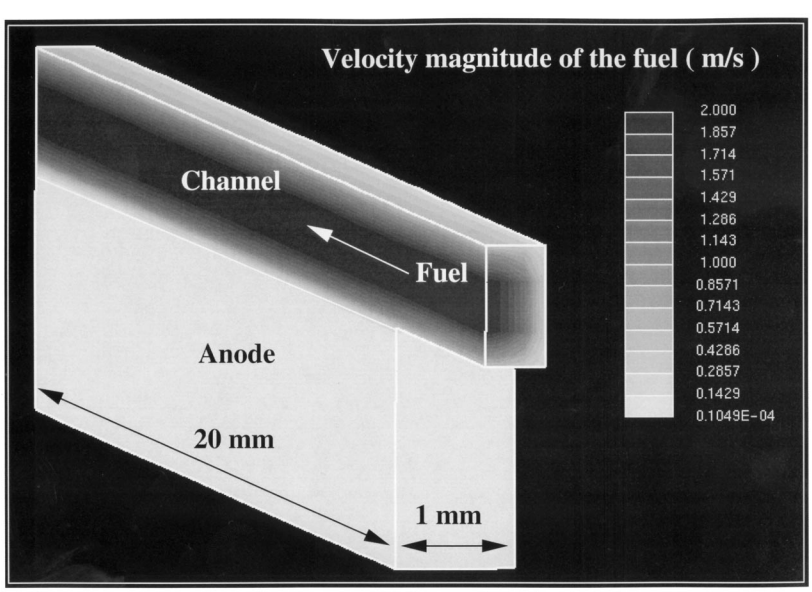

Fig. 3. Calculated profile of the velocity magnitude of the fuel in the channel and the anode.

nature of the anode substrate are listed in Table 2. Fig. 2 shows the schematic diagram of the layout for the concentration polarization measurement. The anode-supported cell was sandwiched between alumina plates with channels. Platinum wire meshes were used as current collectors. The single cell was placed inside an alumina tube in a furnace, and air and fuel gases were fed into the channels from the top and the bottom of the furnace.

3. Results and discussion

From the simulation, it was evident that the velocity magnitude of the fluid gas decreases rapidly in the porous anode. Fig. 3 shows the calculated profile of the velocity magnitude for the fuel flow in the channel and the anode. In this simulation, the mixed gas of $H_2/H_2O = 80/20$ with a velocity of about 2 m/s was introduced from the fuel inlet. One can see that the velocity magnitude of the fuel flow in the anode is reduced to about $1/10^6$ of that in the channel. From the calculated velocity value for the fluid gas in the anode, the H_2 feed rate to the electrolyte by fluid flow is estimated to be about 1×10^{-4} mol m^{-2} s^{-1}. The typical diffusion coefficient of H_2 for the H_2–H_2O binary gas system in the porous anode is about 5×10^{-5} m^2/s. The calculated mole flux of H_2 by diffusion is about 0.23 mol m^{-2} s^{-1}, which is four orders of magnitude higher than that by the flow, and, thus, it can be concluded that the reactant H_2 is mainly transported to the electrolyte by diffusion through the porous anode.

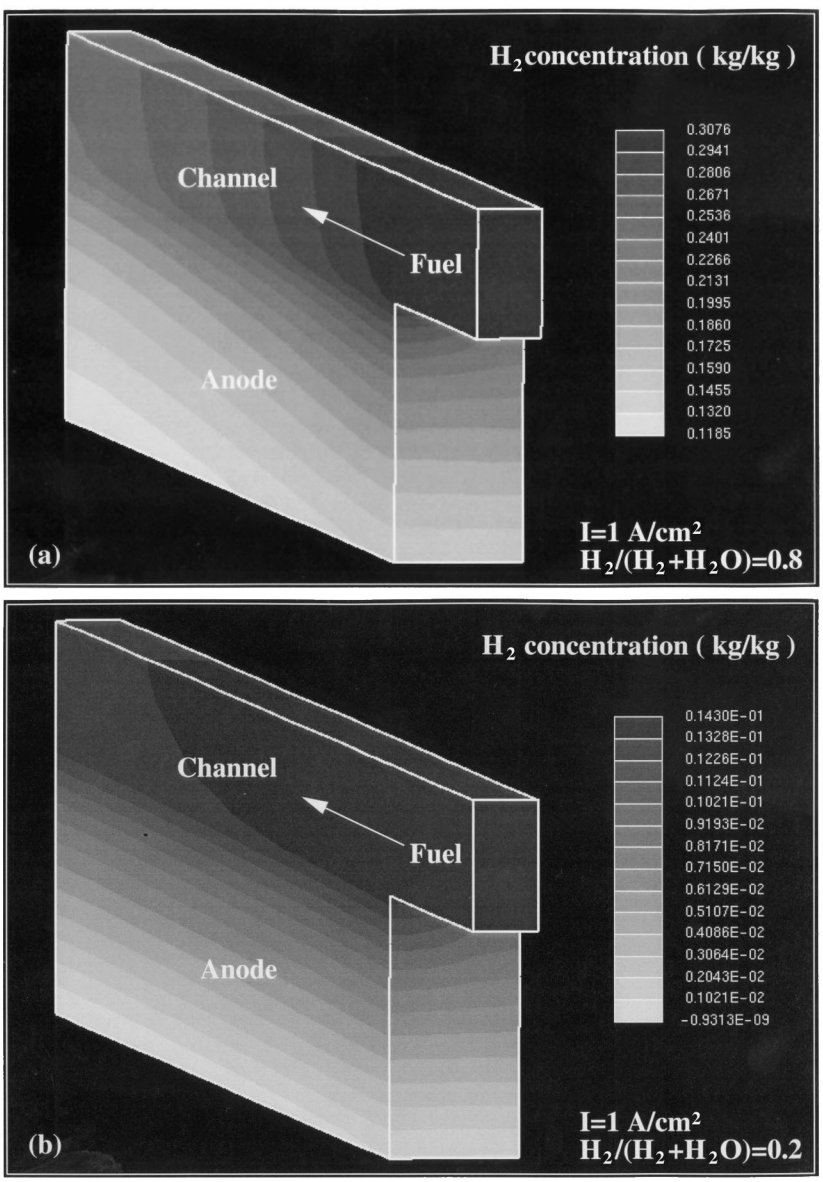

Fig. 4. Calculated distribution of the H_2 concentration in the channel and the anode; (a) for the H_2 concentration of 0.8 and (b) for the H_2 concentration of 0.2.

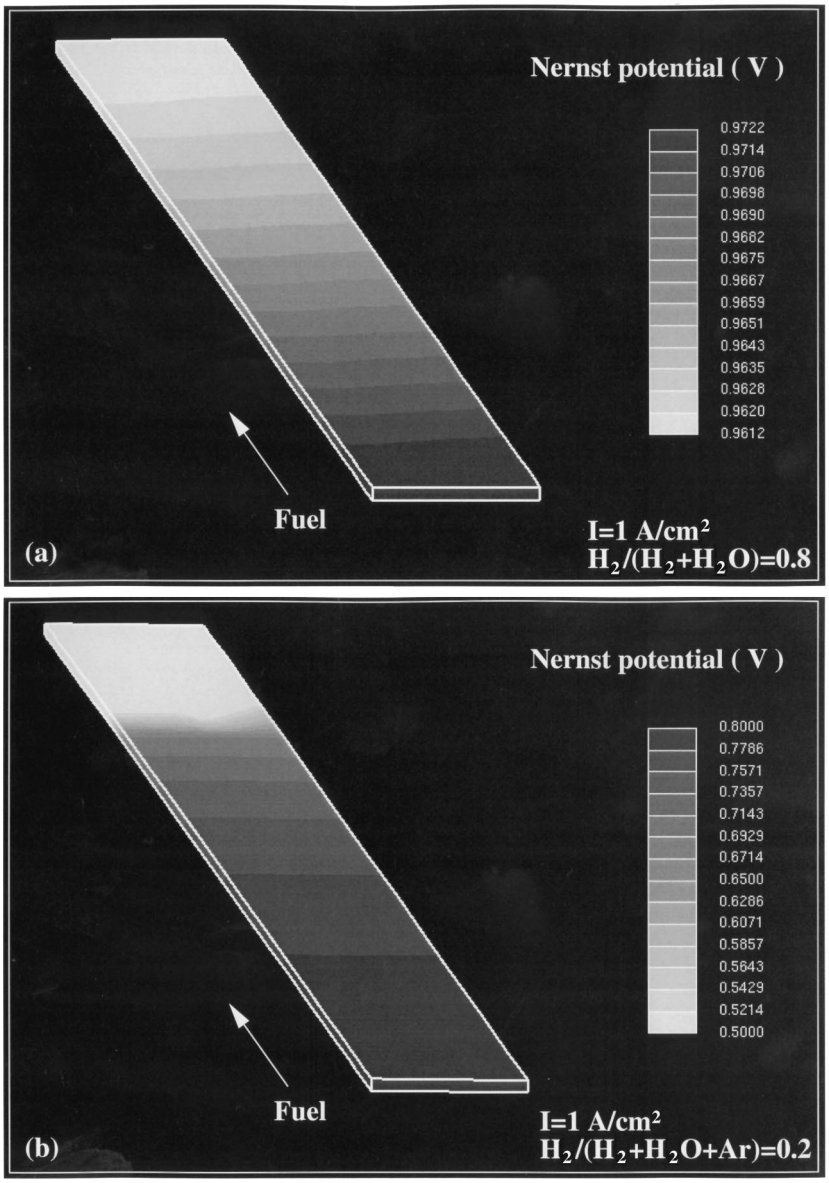

Fig. 5. Calculated Nernst potential profile at the electrolyte/anode interface; (a) for the H_2 concentration of 0.8 and (b) for the H_2 concentration of 0.2.

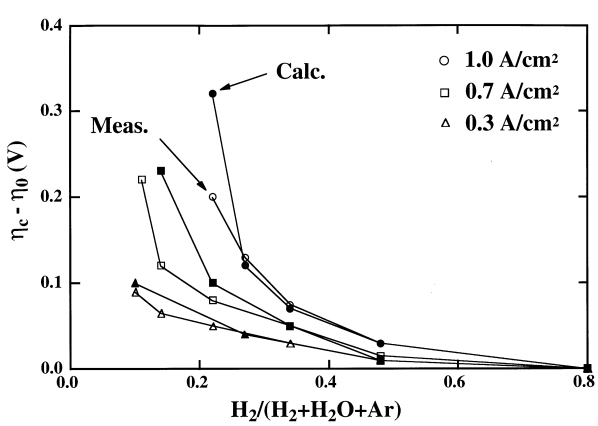

Fig. 6. Comparison of the measured and the calculated concentration overpotential at 0.3, 0.7, and 1.0 A/cm^2 in a H_2–H_2O–Ar system. The open symbols and closed symbols denote the measured and the calculated results, respectively. The solid lines are for a guide to the eyes.

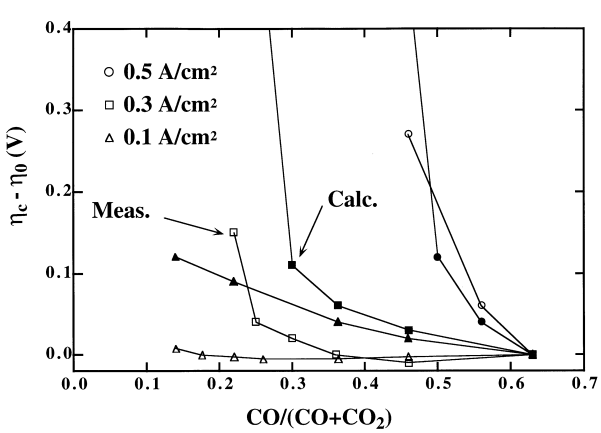

Fig. 7. Comparison of the measured and the calculated concentration overpotential at 0.1, 0.3, and 0.5 A/cm^2 in a CO–CO_2 system. The open symbols and closed symbols denote the measured and the calculated results, respectively. The solid lines are for a guide to the eyes.

The concentration polarization at 0.3, 0.7, and 1.0 A/cm^2 were calculated for the H_2–H_2O–Ar ternary gas system, and compared with experimentally measured values. In these measurements, to keep the open circuit voltage (OCV) constant, the ratio of H_2/H_2O was fixed at 80/20, and the H_2 concentration in the fuel was modified by the degree of dilution of H_2/H_2O gas with Ar gas. The cell operating temperature was kept to 750°C in the measurements, and, correspondingly, the simulation assumed the temperature to be 750°C everywhere in the cell. The velocity of the fuel introduced was set so that the fuel utilization would be less than 5%, which is close to the experimental condition. As well as the cell temperature, the current densities were assumed to be uniform over the entire electrolyte/anode interface.

Fig. 4 exhibits the simulated H_2 concentration profiles in the channel and the anode at 1.0 A/cm^2 for H_2 concentrations of 0.8 and 0.2. In the porous anode, H_2 concentration decreases steadily as the fuel travels from the channel/anode interface to the electrolyte/anode interface. We can see that the gradient of the H_2 concentration along the y direction normal to the electrolyte/anode interface is more gradual near the electrolyte/anode interface than near the channel/anode interface. This is because the diffusion coefficients depend on the gas compositions; the diffusion of H_2 becomes more rapid near the electrolyte/anode interface. The H_2 concentration slightly decreases along the fuel flow path both in the channel and the anode. Although the fuel utilization was chosen to be less than 5%, a slight consumption of H_2 due to oxidation

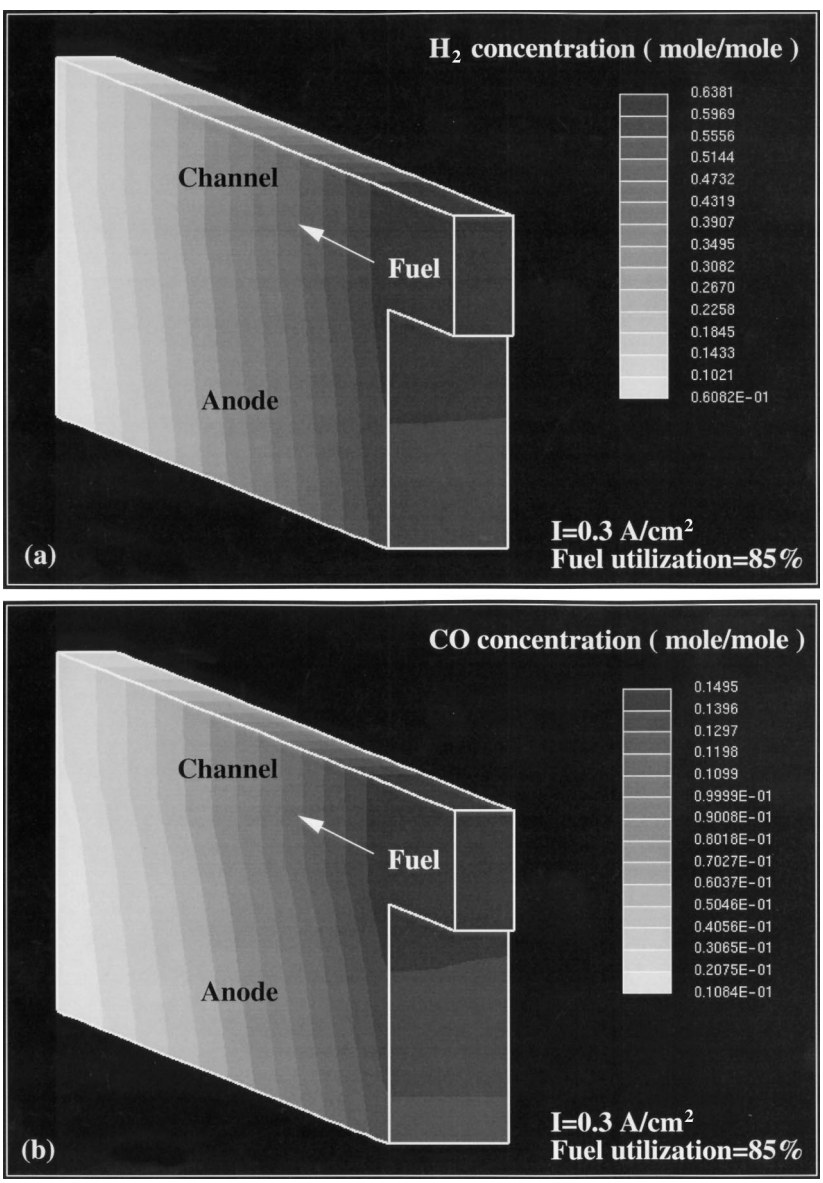

Fig. 8. Calculated distribution of (a) H_2 concentration and (b) CO concentration in the channel and the anode in the methane-reformed gas system.

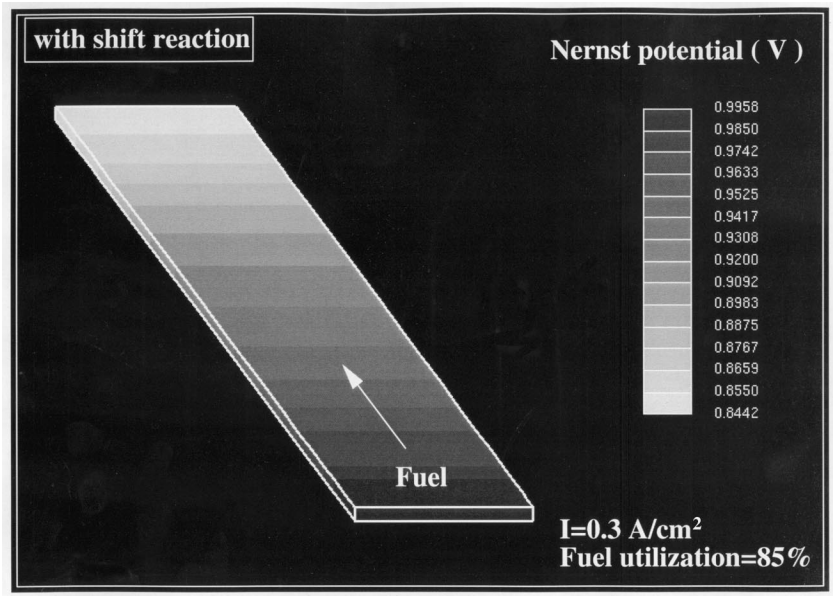

Fig. 9. Calculated Nernst potential profile at the electrolyte/anode interface with consideration of the shift reaction.

causes a decrease of the H_2 concentration along the fuel flow. If the H_2 concentration in the fuel introduced is so low that concentration polarization becomes critical, the enhancement of concentration polarization arising from the slight decrease of the H_2 concentration downstream cannot be neglected; the concentration polarization increases significantly along the fuel flow. Fig. 5 shows the Nernst potential profiles at the electrolyte/anode interface for the H_2 concentration of 0.8 and 0.2, which were calculated from the oxygen partial pressures at the cathode $P_{O_2(c)}$ and the electrolyte/anode interface $P_{O_2(a)}$ at 1.0 A/cm^2. It is seen that, at $H_2/(H_2 + H_2O) = 0.8$, the calculated Nernst potentials show only negligible changes along the fuel flow. At $H_2/(H_2 + H_2O + Ar) = 0.2$, on the other hand, the Nernst potential is seriously reduced with the fuel flow distance, and, thus, an apparent distribution of the Nernst potential appears at the anode. This is because the driving force of $H_2/(H_2 + H_2O + Ar) = 0.2$ is less than that for $H_2/(H_2 + H_2O) = 0.8$ and thus the mole flux H_2 by diffusion is almost the same as the H_2 consumption rate by electrochemical oxidation at the electrolyte/anode interface.

Because the experimentally measured concentration overpotential is the average value over the anode, the distribution of η_c at the anode will exhibit an increase in the η_c vs. $H_2/(H_2 + H_2O + Ar)$ plot, which is less steep.

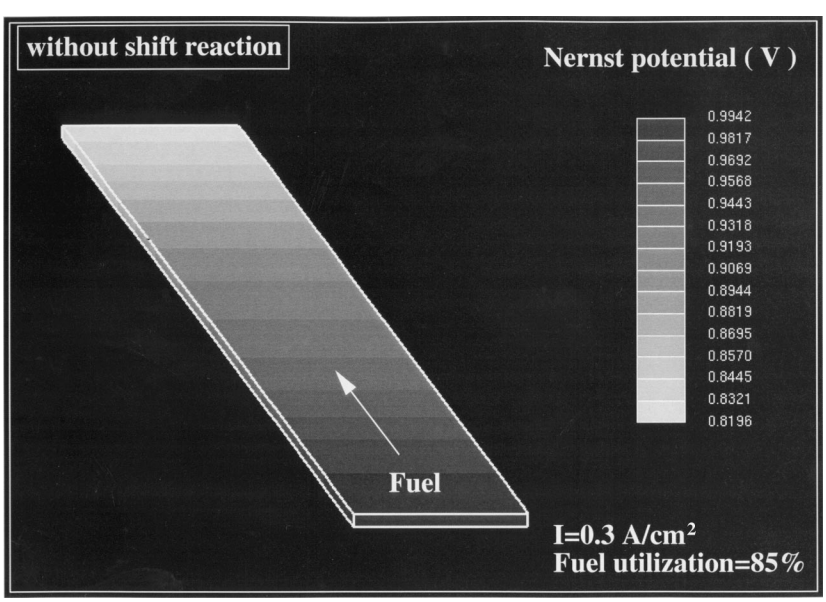

Fig. 10. Calculated Nernst potential profile at the electrolyte/anode interface without consideration of the shift reaction.

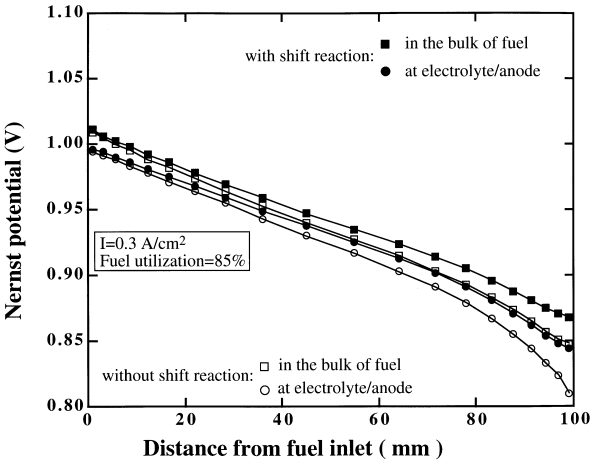

Fig. 11. Comparison of the calculated Nernst potentials along the fuel flow with and without consideration of the shift reaction. The filled and open symbols denote the results with and without consideration of the shift reaction, respectively.

Fig. 6 shows the comparison of the measured and the simulated η_c in the H_2–H_2O–Ar system. For the calculated results, the distribution of η_c at the anode was taken into consideration, and the average values over the anode were employed. In Fig. 6, $\eta_c - \eta_0$, where η_0 is the concentration overpotential at $H_2/(H_2 + H_2O) = 0.8$, is plotted as a function of the H_2 concentration for various current densities. In the simulation, only the tortuosity was treated as a variable parameter, and selected as 4.5 to fit the experimentally measured results at 1 A/cm^2. From Fig. 6, it was found that the present model well simulates the rise in the η_c vs. $H_2/(H_2 + H_2O + Ar)$ plots. As can be seen in the plot, the rise of η_c with decreasing H_2 concentration in the fuel introduced is not so sharp for both the measured and the simulated results, which might reflect the above-mentioned η_c distribution at the anode.

For a CO–CO_2 system, η_c is large even at lower current densities as compared with the H_2–H_2O system, since the diffusion rate of reactant CO in the CO–CO_2 system is lower than that of H_2 in the H_2–H_2O system. Fig. 7 shows the comparison of the measured and the simulated $\eta_c - \eta_0$ for the CO–CO_2 binary system, where η_0 is the concentration overpotential at $CO/(CO + CO_2) = 0.64$. Similar to the simulation for the H_2–H_2O system, the calculated η_c is the average value over the anode. Although the magnitude of the calculated $\eta_c - \eta_0$ is larger than the experimentally measured results when the current density is 0.3 or 0.1 A/cm^2, the critical CO concentration at which the concentration polarization increases steeply shows good agreement between the simulation and the experiments. Even at a moderate current density of 0.3 A/cm^2, we can see a steep increase of $\eta_c - \eta_0$ when decreasing the CO concentration to less than 0.2 for both the simulated and the measured results. This means that if a fuel gas contains only CO as the reactant, the concentration polarization must be serious at a high fuel utilization of over 80%, even at 0.3 A/cm^2. Hence, the fuel utilization should be carefully controlled when a fuel containing CO is used.

The simulation for a multicomponent system where a methane-reformed gas is used as the fuel is considered next. In a methane-reformed gas system, the concentration polarization at a high fuel utilization must be significant because the methane-reformed gas contains much CO as reactant. For the methane-reformed gas system, it has been reported that the electrochemical oxidation rate of H_2 is about two times higher than that of CO [9], and, thus, more H_2 is consumed than CO at the electrolyte/anode inter-

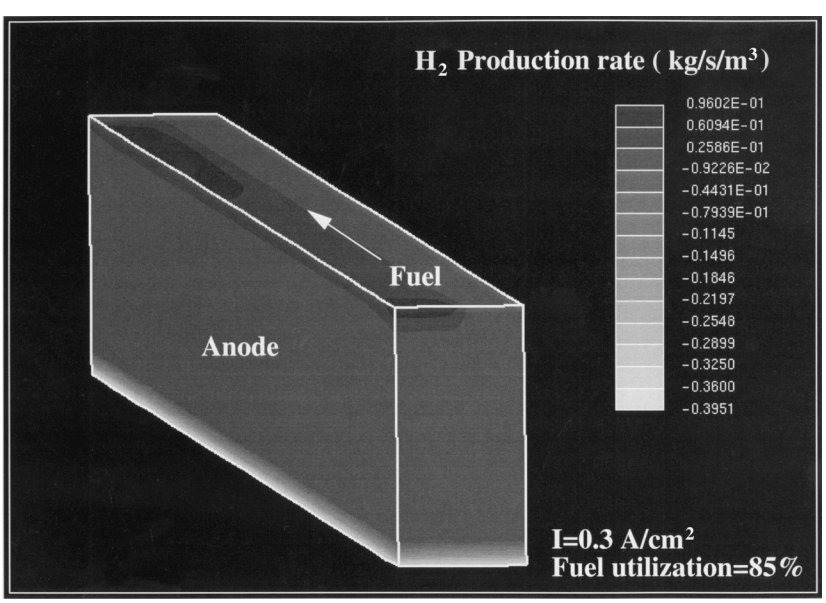

Fig. 12. H_2 production or consumption rate in the anode. The shift reaction was taken into account.

face. Besides, the diffusion of H_2 is about two times faster than that of CO. As a result, H_2 diffuses selectively to the electrolyte/anode interface from the channel/anode interface, and the relative concentration of H_2 to CO in the channel will become lower downstream. When the fuel utilization is high, H_2 will be depleted even in the fuel channel downstream while CO is not depleted in this channel. In addition, a depletion of CO at the electrolyte/anode interface will occur because of the slower CO diffusion rate. Thus, the concentration polarization will be critical for the fuel circuit downstream even though there is enough CO in the channel.

In the present calculation, the fuel gas contains $CH_4 = 0.005$ (%), $H_2O = 15.9$ (%), $H_2 = 63.8$ (%), $CO = 14.9$ (%), and $CO_2 = 4.76$ (%), which corresponds to the equilibrium composition of a mixture of CH_4 and steam at $H_2O/CH_4 = 2$. The current density of 1 A/cm^2 was assumed to be uniform everywhere at the electrolyte/anode interface, as in the study for the H_2–H_2O and CO–CO_2 systems, whereas, the fuel utilization was selected to be 85%, which is significantly higher than in the simulation for the binary gas systems. At such a high fuel utilization, the concentrations of the reactant gases are found to be low even in the channel, as illustrated in Fig. 8, and, thus, the Nernst potential decreases in the fuel flow direction. In Fig. 9, the Nernst potential profile calculated from $p_{O_2(c)}$ and $p_{O_2(a)}$ is exhibited, and the Nernst potential in the fuel path downstream is considerably lower than that for the fuel upstream. The important point to note here is that the shift reaction effectively hinders the depletion of the reactant gases downstream. Fig. 10 exhibits the calculated Nernst potential profile at the electrolyte/anode interface when the shift reaction is not taken into account. Compared to the results with and without consideration of the shift reaction, it is found that the difference of the Nernst potential downstream cannot be neglected. Fig. 11 exhibits the comparison of the calculated Nernst potentials along the fuel flow direction with and without consideration of the shift reaction. It is obvious that the Nernst potentials, which consider the shift reaction, are higher than those which do not consider the shift reaction, especially downstream. Besides, the concentration polarization downstream is reduced when the shift reaction is taken into account. The higher Nernst potential and the lower concentration polarization, which account for the shift reaction, can be attributed to production of H_2 in the fuel path downstream. Fig. 12 shows the production or consumption rate of H_2 in the anode. Much H_2 is produced by the shift reaction near the channel/anode interface, and the H_2 produced is transported by diffusion and supplied to the electrolyte. The shift reaction is, thus, effective in preventing the depletion of the reactant gases near the electrolyte/anode interface.

4. Conclusions

A single-unit model with double channels of a counter-flow pattern was constructed for an anode-supported SOFC. The flow and electrochemical phenomena in the H_2–H_2O–Ar, CO–CO_2, and the methane reformed gas systems were simulated, and the concentration overpotential at the anode was calculated. For the H_2–H_2O–Ar and CO–CO_2 systems, the calculated concentration overpotential was in good agreement with the experimentally measured results. For the methane-reformed gas system, it was apparent that the concentration polarization increases considerably along the fuel flow path at a high fuel utilization. The shift reaction was found to effectively reduce the concentration polarization.

References

[1] H.P. Buchkremer, U. Diekmann, L.G.J. de Haart, H. Kabs, D. Stöver, I.C. Vinkel, in: P. Stevens (Ed.), Proceedings of the 3rd European Solid Oxide Fuel Cell Forum, Nantes, France, 1998, p. 143.
[2] J.W. Kim, A.V. Virkar, K.N. Fung, K. Mehta, S.C. Singhal, J. Electrochem. Soc. 146 (1999) 69.
[3] A. Reizes, Transport Phenomena in Heat and Mass Transfer, Elsevier, Amsterdam, 1992.
[4] M. Asaeda, M. Nakano, R. Toei, J. Chem. Eng. Jpn. 7 (1974) 173.
[5] J. Kestin, W.A. Wakeham, Transport Properties of Fluids; Thermal conductivity, Viscosity, and Diffusion Coefficient, Hemisphere Publishing, New York, 1988.
[6] R. C Reid, J.M. Prausnitz, T.K. Sherwood, The Properties of Gases and Liquids, McGraw-Hill, New York, 1977.
[7] P.D. Neufeld, A.R. Janzen, R.A. Aziz, J. Chem. Phys. 57 (1972) 1100.
[8] U.R. Hattikudur, G. Thodos, J. Chem. Phys. 52 (1970) 4313.
[9] Y. Matsuzaki, I. Yasuda, will be published in Proceedings of Solid Oxide Fuel Cells VI, Honolulu, HI, October 17–22, 1999.